Equation of state for a partially ionized gas. III

George A. Baker, Jr.
Theoretical Division, Los Alamos National Laboratory, Los Alamos, New Mexico 87544, USA
(Received 18 October 2007; published 18 March 2008)

The derivation of equations of state for fluid phases of a partially ionized gas or plasma is addressed from a fundamental point of view. The results of the Thomas-Fermi model always yield pressures which are less than or equal to that of an ideal Fermi gas. On the other hand, the spherical cellular model shows significant "overpressure" relative to the ideal Fermi gas in certain regions of low density and low temperature. This effect is studied in considerable detail. A nonthermodynamic region, more or less overlapping the regions of overpressure, is found. It is characterized by a negative specific heat at constant volume. An independent electron model within a Z-electron cell is employed. The inadequacy of the wave function in the low-density, low-temperature nonthermodynamic region is shown to be the cause of this overpressure. Numerical examples of the theory for several elements (Li, N, Al, K, and Er) are reported. These results reduce in various limits of temperature and density to the expected behavior, except in the aforementioned region.

DOI: 10.1103/PhysRevE.77.031120 PACS number(s): 05.30.−d, 51.30.+i, 05.70.Ce, 64.10.+h

I. INTRODUCTION AND SUMMARY

In a series of papers [1,2] I have investigated from a fundamental point of view the thermodynamic properties of ion-electron systems with emphasis on the single-phase region. (There was a miscoding in [2] which was corrected in [3].) This series of papers has, for a starting point, the observation that the exact solution for the ideal gas can be reformulated in terms of calculations in a cubic cell (or for that matter for any cell of a Bravais lattice). The next step was the approximation of using a spherical cell instead. For nuclear charge greater than unity, an independent electron model is used. A list of all the approximations is given in Appendix B of [2]. In this paper, and in the previous ones, the dipole-dipole interaction will not be considered. A discussion of a large number of alternative approaches is given in [1]. In addition, in collaboration with Johnson, I have studied some of the thermodynamic quantities in terms of a series expansion in the electron charge e about the ideal Fermi gas [4–6]. (The above-mentioned miscoding affected some of the numerical results in [6]. These were corrected in [7].

The most popular of the alternative approaches is probably the Thomas-Fermi model [8–13] and its Thomas-Fermi-Dirac extension [14,15] which includes the exchange interaction. In this paper I notice that the Thomas-Fermi model always produces pressures that are less than or equal to the ideal, Fermi gas pressure. On the other hand, the spherical cellular model in certain cool, dilute regions produces pressures that significantly exceed the ideal gas pressure. This effect has been proven to be possible [16] for certain density-dependent potentials. I investigate this phenomenon in some detail.

In Sec. II, I give a brief summary of the formulation of the cellular model. In Sec. III, I illustrate some examples of cases where the pressure computed for the spherical cellular model is much greater than the ideal gas pressure. This result is contrasted with those of the Thomas-Fermi model, which never gives a pressure higher than the ideal gas. In Sec. IV, I find that a negative specific heat is generated in some regions by the spherical cellular model. I give a construction, which is analogous to the Maxwell construction, to delineate the nonthermodynamic region. In Sec. V, I review some of the behaviors of various quantities which are computed from the spherical cellular model and are relevant to the "overpressure" and the nonthermodynamic behavior of this model. In the last section, I conclude that (i) the very large overpressures seem to occur mainly in the nonthermodynamic region and so are not physical; (ii) there is a rather large region where the spherical cellular model can be expected to provide a reasonable approximation to the proper equation of state; and (iii) the spherical cellular model for hydrogen has no nonthermodynamic regions.

II. FORMULATION OF THE CELLULAR MODEL

In a previous paper [1] I pointed out that one can divide all space into cubical cells. The reciprocal lattice is again cubic. For the ideal Fermi gas, if one sums over all the eigenvalues of the Hamiltonian in a cell and integrates over the first Brillouin zone, this procedure amounts to a simple rearrangement of the integrals in the usual formulation [17] of the exact solution for the thermodynamic properties of the ideal Fermi gas. The boundary conditions for the determination of the eigenvalues are the usual ones, i.e., the wave function and its derivative are continuous at the surface of the cell. The cells in this cellular model are stacked and have the same wave function inside each cell, which gives meaning to the continuity conditions just stated.

The quantum statistical mechanics formulas on which the usual formulation is based are given for Fermi-Dirac statistics. The grand canonical partition function is

$$\mathcal{Q}(\Omega,T)=\sum_{\mathcal{N}=0}^{\infty}\exp[\mathcal{N}\mu(\Omega,T)/(kT)]Q_{\mathcal{N}}(\Omega,T)$$
$$=\prod_{j}\left(1+\exp\{[\mu(\Omega,T)-\epsilon_j]/(kT)\}\right), \quad (2.1)$$

where Ω is the volume, T is the absolute temperature, the ϵ_j's are the state energies, and k is Boltzmann's constant. Differ-

entiating by μ (the chemical potential) determines μ as the solution of

$$\mathcal{N} = \sum_j \frac{1}{\exp[(\epsilon_j - \mu)/(kT)] + 1}, \tag{2.2}$$

where $\mathcal{N}$ is the average number of occupied states. The Helmholtz free energy is then given as

$$A(\Omega, T) = \mathcal{N}\mu(\Omega, T) - kT\sum_j \ln(1 + \exp\{[\mu(\Omega, T) - \epsilon_j]/(kT)\}). \tag{2.3}$$

From it, one can deduce the pressure and internal energy as

$$p\Omega = -\frac{1}{3} r_b \left.\frac{\partial A}{\partial r_b}\right|_T = -\frac{1}{3}\sum_j \frac{r_b \left.\frac{\partial \epsilon_j}{\partial r_b}\right|_T}{\exp[(\epsilon_j - \mu)/(kT)] + 1}, \tag{2.4}$$

$$U = A - T \left.\frac{\partial A}{\partial T}\right|_\Omega = \sum_j \frac{\epsilon_j - T \left.\frac{\partial \epsilon_j}{\partial T}\right|_\Omega}{\exp[(\epsilon_j - \mu)/(kT)] + 1}, \tag{2.5}$$

where r_b characterizes the linear size of the cell. For a spherical cell, it is the radius of the sphere.

Specifically the usual formulation of the ideal Fermi gas is, with $Z=1$,

$$\zeta = \frac{ZN}{2\Omega}\left(\frac{h^2}{2\pi mkT}\right)^{3/2} = f_{3/2}(z) = \frac{2}{\sqrt{\pi}}\int_0^\infty \frac{zy^{1/2}e^{-y}dy}{1 + ze^{-y}}, \tag{2.6}$$

where ζ is the de Broglie density, ZN is the number of electrons, z is the fugacity, h is Planck's constant, and m is the electron mass. The pressure p is given by

$$\frac{p\Omega}{ZNkT} = \frac{f_{5/2}(z)}{f_{3/2}(z)}, \quad f_{5/2}(z) = \frac{4}{3\sqrt{\pi}}\int_0^\infty \frac{zy^{3/2}e^{-y}dy}{1 + ze^{-y}}. \tag{2.7}$$

Let us reexpress these equations in terms of $y = \hbar^2\vec{k}^2/(2mkT)$ and $a^3 = \Omega/(ZN)$. The primitive-cell edge in the reciprocal lattice is $2\pi/a$. If one does some re-arranging of the integrals, then (2.6) becomes

$$1 = 2\sum_{j_1=-\infty}^{+\infty}\sum_{j_2=-\infty}^{+\infty}\sum_{j_3=-\infty}^{+\infty}\left(\frac{a}{2\pi}\right)^3 \times \int\int\int_{-\pi/a}^{\pi/a} \frac{d\vec{k}}{1 + z^{-1}\exp\left[\frac{\hbar^2}{2mkT}\left(\vec{k} + \frac{2\pi}{a}\vec{\mathcal{J}}\right)^2\right]}, \tag{2.8}$$

where the steps in $\vec{\mathcal{J}}$ are unity. Equation (2.7) becomes

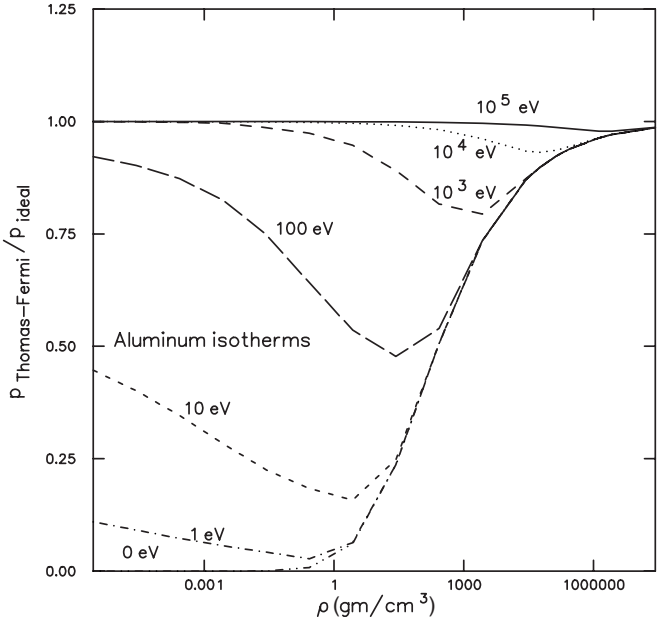

FIG. 1. Thomas-Fermi model pressure divided by the ideal gas pressure vs density for the case of aluminum ($Z=13$).

$$\frac{p\Omega}{ZNkT} = 2\sum_{j_1=-\infty}^{+\infty}\sum_{j_2=-\infty}^{+\infty}\sum_{j_3=-\infty}^{+\infty}\left(\frac{a}{2\pi}\right)^3 \times \int\int\int_{-\pi/a}^{\pi/a} \frac{\frac{\hbar^2}{2mkT}\left(\vec{k} + \frac{2\pi}{a}\vec{\mathcal{J}}\right)^2 d\vec{k}}{1 + z^{-1}\exp\left[\frac{\hbar^2}{2mkT}\left(\vec{k} + \frac{2\pi}{a}\vec{\mathcal{J}}\right)^2\right]}. \tag{2.9}$$

In that same paper [1], there is an investigation of the use of spherical cells instead of cubic cells (or for that matter cells based on any Bravais lattice). Since the term $-i\hbar^2\vec{k}\cdot\vec{\nabla}$ which arises in the Hamiltonian is not diagonal in spherical coordinates, a certain additional approximation is required by numerical expediency. See [1], Sec. IV. The results are that the pressure for the ideal Fermi gas is accurate to within about −2.2 to 4.9%. Some additional modifications were made to ensure that the leading-order corrections to the ideal gas results are given correctly and to account for the exchange effects. These equations can be used to investigate the behavior of various thermodynamic quantities for hydrogen.

In order to proceed to various other elements, the direct application of these ideas results in having Z (more than one) electrons in each cell with a single nucleus of charge $+Ze$. The direct generalization of [1] (5.1) leads to the equation

$$\left[\sum_{j=1}^{Z}\left(\frac{\hbar^2}{2m}(k^2 - 2i\vec{k}\cdot\vec{\nabla}_j - \nabla_j^2) - \frac{Ze^2}{r_j}\right) + \frac{1}{2}\sum_{l\neq j}^{Z}\frac{e^2}{|\vec{r}_l - \vec{r}_j|}\right]\phi_{l,\lambda}(\vec{r}_1, \ldots, \vec{r}_Z) = E_{l,\lambda}\phi_{l,\lambda}(\vec{r}_1, \ldots, \vec{r}_Z), \tag{2.10}$$

where $\vec{\nabla}_j$ means differentiation with respect to $\vec{r}_j$. The same

value of $\vec{k}$ is used in $\exp(i\vec{k}\cdot\vec{r}_j)$ for all $\vec{r}_j$ in order to maintain the antisymmetry of the wave function.

These problems (2.10) are numerically intractable, so in [2] the independent electron approximation is introduced. The equations now become

$$\left[\frac{\hbar^2}{2m^*}(k^2-2i\vec{k}\cdot\vec{\nabla}-\nabla^2)-\frac{e^2Z^{-1/3}v(r_b,T,r/r_b)}{r}-\frac{e^2Z^{-1/3}}{2r_b}\left(\frac{r}{r_b}\right)^2F\left(\frac{y^2}{Z}\right)\right]\phi_{l,\lambda}(\vec{r})=\mathcal{E}_{l,\lambda}(\vec{k})\phi_{l,\lambda}(\vec{r}), \tag{2.11}$$

with the boundary conditions

$$\vec{n}\cdot\vec{\nabla}\phi_{\text{even}}(Z^{1/3}\vec{\hat{r}}_b)=0,\quad \phi_{\text{odd}}(Z^{1/3}\vec{\hat{r}}_b)=0, \tag{2.12}$$

where $\vec{n}$ is the unit vector normal to the sphere.

$$\hat{r}_b=\left(\frac{3\mathcal{A}}{4\pi\mathcal{N}_0Z\rho}\right)^{1/3}=7.344\,995\times10^{-9}\left(\frac{\mathcal{A}}{Z\rho}\right)^{1/3}\ \text{cm}, \tag{2.13}$$

where $\mathcal{A}$ is the gram atomic weight, $\mathcal{N}_0$ is Avogadro's number, and $y^2=Ze^2/(r_bkT)$ is a dimensionless strength of the Coulomb interaction. $\hat{r}_b$ is the radius of the spherical cell r_b over $Z^{1/3}$. The effective mass m^* is defined in [1]. The F term relates to the electron-electron repulsion. For an alternate approach, see, for example, [18]. In the spherical cell approximation, the normalization condition that determines the chemical potential $\mu=kT\ln z$ is

$$1=3\sum_{l=0}^{\infty}(2l+1)\sum_{n=0}^{\infty}\int_0^1 d\hat{\kappa}\,\hat{\kappa}^2\left(\frac{1}{1+\exp\{(1.5\sqrt{\pi}\zeta)^{2/3}[e_{l,n}+(1/2)(1+m^*/m)(\hat{\kappa}^2+\hat{\kappa}\hat{\Delta}_{n+[(l+1)/2]})]-\mu/kT\}}+\frac{1}{1+\exp\{(1.5\sqrt{\pi}\zeta)^{2/3}[e_{l,n}+(1/2)(1+m^*/m)(\hat{\kappa}^2-\hat{\kappa}\hat{\Delta}_{n+[(l+1)/2]})]-\mu/kT\}}\right), \tag{2.14}$$

where now the dimensionless form of the eigenvalue is

$$e_{l,n}=\frac{2m\epsilon_{l,n}(\vec{0})}{\hbar^2k_B^2}, \tag{2.15}$$

where $k_B=(9\pi/2)^{1/3}/r_b$. The $\hat{\Delta}_{n+[(l+1)/2]}$ are defined in [1]. For the corresponding ϵ,

$$\epsilon_{l,\lambda}(\vec{k})=\frac{1}{2}\left(1+\frac{m^*}{m}\right)\left[\mathcal{E}_{l,\lambda}(\vec{k})-\frac{1}{2}\langle\phi_{l,\lambda}(\vec{r})|\left(\frac{Z^{2/3}e^2}{r}-\frac{e^2v(r_b,T,r/r_b)Z^{-1/3}}{r}\right)|\phi_{l,\lambda}(\vec{r})\rangle\right]-\frac{1}{2}\left(1-\frac{m^*}{m}\right)\langle\phi_{l,\lambda}(\vec{r})|\frac{v(r_b,T,r/r_b)e^2Z^{-1/3}}{r}|\phi_{l,\lambda}(\vec{r})\rangle+\frac{m^*e^2Z^{-1/3}}{4mr_b}F\left(\frac{y^2}{Z}\right)\langle\phi_{l,\lambda}(\vec{r})|\frac{r^2}{r_b^2}|\phi_{l,\lambda}(\vec{r})\rangle+\Delta\epsilon. \tag{2.16}$$

where the state-independent part is

$$\Delta\epsilon_{\parallel}=Z^{-1/3}\left\{\frac{3e^2}{10r_b}g(y^2)+\frac{3Ze^2}{5r_b}F(y^2Z)+\frac{e^2}{r_b}F\left(\frac{y^2}{Z}\right)\left[\frac{3}{4}-\left(\frac{3Z}{\pi\zeta}\right)^{1/3}f_{1/2}(z(\zeta))\right]\right\},$$

$$\Delta\epsilon_{\text{anti-}\parallel}=Z^{-1/3}\left[\frac{3e^2}{10r_b}g(y^2)+\frac{3Ze^2}{5r_b}F(y^2Z)+\frac{3e^2}{4r_b}F\left(\frac{y^2}{Z}\right)\right]. \tag{2.17}$$

For the antiparallel case $m^*/m=1$ and I drop the $f_{1/2}$ term. m^*, as explained in [1], is the effective mass in the parallel spin case. Account has been taken of the double counting of the electron-electron interactions.

The potential is determined self-consistently by the use of Poisson's equation, which leads to

$$v(r_b,T,r/r_b)=1+\left(\frac{Z-1}{Z}\right)r_b\int_{(r/r_b)}^1\left(1-\frac{r}{\beta r_b}\right)\mathcal{D}(r_b,T,\beta)d\beta. \tag{2.18}$$

$\mathcal{D}(r_b,T,\beta)$ is the electron density. For the case of a uniform density $\mathcal{D}(r_b,T,r/r_b)=3Zr^2/r_b^3$, and $v(r_b,T,r/r_b)=Z+\frac{1}{2}(Z-1)[(r/r_b)^3-3(r/r_b)]$. I use this value to start the iteration procedure to find the solution of these equations. The full details are found in [2], and Appendix B of that paper gives a catalog of all the approximations.

III. OVERPRESSURES

As has been noticed (see, for example, [19]), the pressure of the Thomas-Fermi model is always less than or equal to that of the ideal gas, as seen in Fig. 1. It is sufficient to consider just one element for this purpose because of the similarity considerations derived in [10]. On the other hand, the pressure computed for the spherical cellular model is

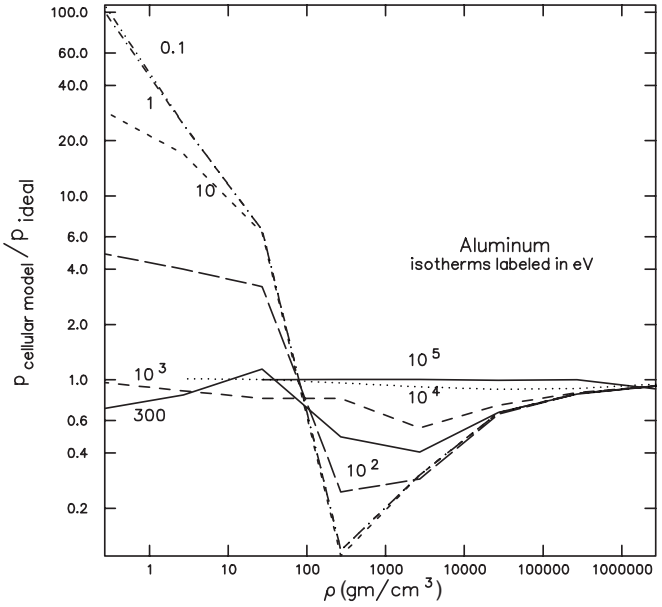

FIG. 2. Spherical cellular model pressure divided by the ideal gas pressure vs density for the case of aluminum ($Z=13$).

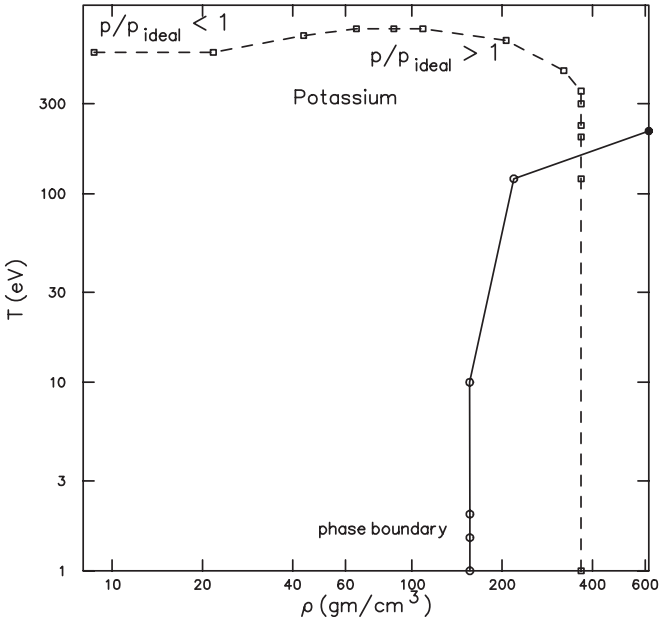

FIG. 3. Spherical cellular model plot of the temperature vs the density of the boundary of the region where the pressure is greater than that the ideal gas. Also plotted is the phase boundary of the two-phase region.

sometimes greater and occasionally considerable greater than that of the ideal gas, as seen in Fig. 2. This overpressure merits considerable investigation to see whether it is an artifact of the theory, or reflects real behavior. There are some experimental results [20] on aluminum for $\rho=0.1$ and 0.3 gm/cm^3 at temperatures of a few eV. They indicate a system of very little ionization with the pressure less than that of an ideal gas of ions and electrons. This effect does not occur in hydrogen. The overpressure effect does not occur exclusively in the two-phase region. This fact is illustrated in Fig. 3, which shows for potassium the $p=p_{\text{ideal}}$ line and the phase boundary. To study this situation for $Z>1$, I have plotted the internal energy vs the temperature for fixed density. One example is given by in Fig. 4. A further example is given by the isotherms of the spherical cellular model showing the internal energy versus volume for lithium (Fig. 5). Notice that, while the 3 eV isotherm is higher than the others for low volume, it is lower than the others for high volume.

IV. CONSTRUCTION

An analogous situation occurs in the study of the van der Waals equation of state. Here when the pressure is plotted versus the volume there is a violation of the thermodynamic requirement that $\partial p/\partial V|_T \leq 0$. The solution to this problem is the Maxwell construction. This condition is imposed by the insertion of a line of constant pressure which connects two points (points 1 and 2) on the van der Waals curve. The requirements are that $p(V_1)=p(V_2)$ and that there is no net work done. That is to say, $\int_{V_1}^{V_2} p\, dV=0$, the famous equal-areas law.

In the case illustrated in Fig. 4 there is a negative specific heat at constant density (volume), which is a violation of thermodynamics as the specific heat at constant volume C_V is a principal specific heat. I propose an analogous construction to that of Maxwell. First, note the thermodynamic relations

$$\left.\frac{\partial A}{\partial T}\right|_V = -S, \qquad \left.\frac{\partial U}{\partial T}\right|_V = T\left.\frac{\partial S}{\partial T}\right|_V = C_V = -T\left.\frac{\partial^2 A}{\partial^2 T}\right|_V, \tag{4.1}$$

where U is the internal energy, and S is the entropy. The condition that no work be done is that $U(T_1,V)=U(T_2,V)$. The condition that the slopes of the Helmholz free energy A

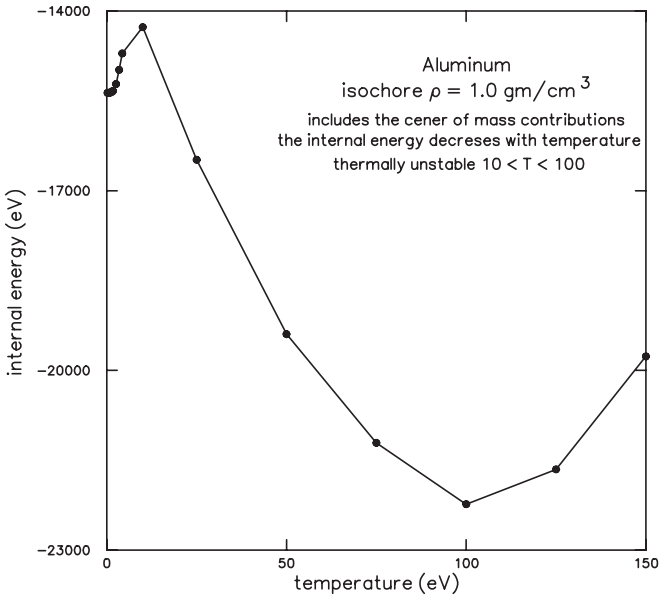

FIG. 4. Spherical cellular model internal energy for $\rho=1$ as a function of temperature.

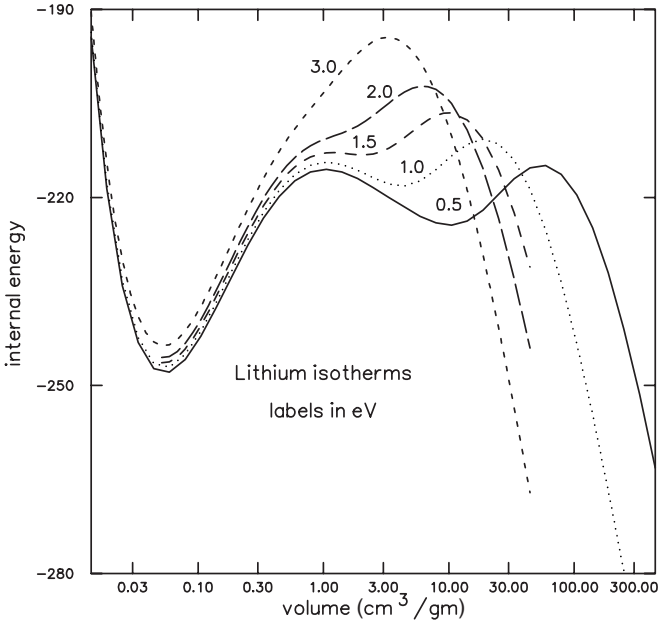

FIG. 5. Spherical cellular model lithium isotherms showing the internal energy as a function of volume, reflecting the nonthermodynamic region.

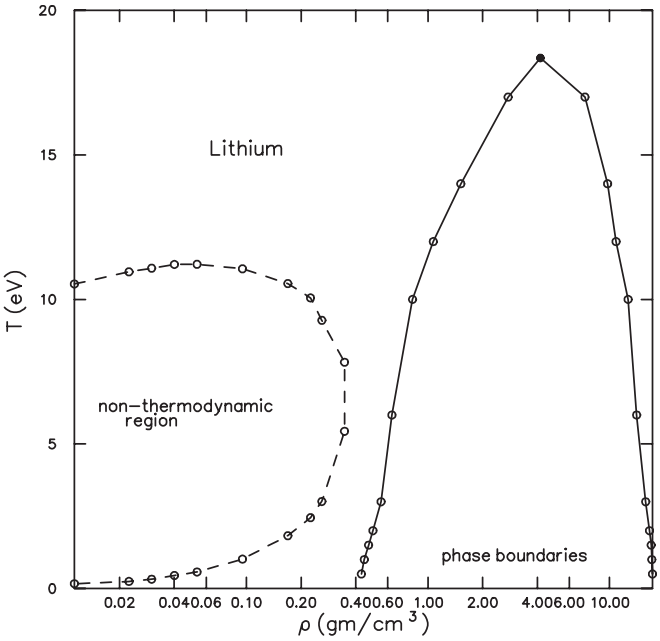

FIG. 6. Spherical cellular model for lithium showing, as a function of volume and temperature, the nonthermodynamic region.

with respect to temperature be equal is $S(T_1,V)=S(T_2,V)$, or

$$\int_{T_1}^{T_2} \frac{dt}{t} \left. \frac{\partial U(t,V)}{\partial t} \right|_V = 0. \tag{4.2}$$

(Note that this latter condition is independent of an additive constant to the internal energy so I do not need to invoke the third law of thermodynamics.) These conditions, in a way analogous to the Maxwell construction, define a region in which the spherical cellular model behaves in a nonthermodynamic fashion. I illustrate this for lithium in Fig. 6. The boundaries of the nonthermodynamic regions seem to collapse when plotted as a function $Z^{0.2}y$ of ζ. See Fig. 7. Hydrogen is an exception as it does not have a nonthermodynamic region. There is some indication from the results for lithium that values of ζ greater than some minimum value do not show nonthermodynamic behavior. For lithium this value is about 8. That is to say, for a fixed value of ζ greater than a certain value, no y will be in a nonthermodynamic region. Likewise, referring to Fig. 6 for any fixed ρ for T greater than a certain value, there will not be any nonthermodynamic regions. I expect that results of this character will be valid for the other elements as well. This idea is in line with the fact that for very high densities and/or very high temperatures the kinetic energy is much more important than the potential energy.

V. BEHAVIOR OF THE SPHERICAL CELLULAR MODEL

It is not that the pressure behaves wildly in the spherical cellular model. On the contrary, it sometimes simply fails to drop as expected when the temperature decreases at fixed density. I illustrate this in Fig. 8. Since Fig. 8 is at constant density, i.e., constant volume, the low-temperature limit of the pressure can be thought of as proportional to $\langle r_b[\partial \epsilon_1(\vec{0})]/[\partial r_b]\rangle$, which is clearly too large. As I have shown in Fig. 18 of [2] for low densities, $r_b \partial v(r_b,T,r/r_b)/\partial r_b$ is positive. Thus I expect, and I do find, $p/p_{\text{ideal}}>1$. For high densities, on the other hand, this quantity is negative, in line with $p/p_{\text{ideal}}<1$.

The general pattern is seen for all the elements I have checked (except for hydrogen where the nonthermodynamic region does not appear). The curves for the boundaries of the

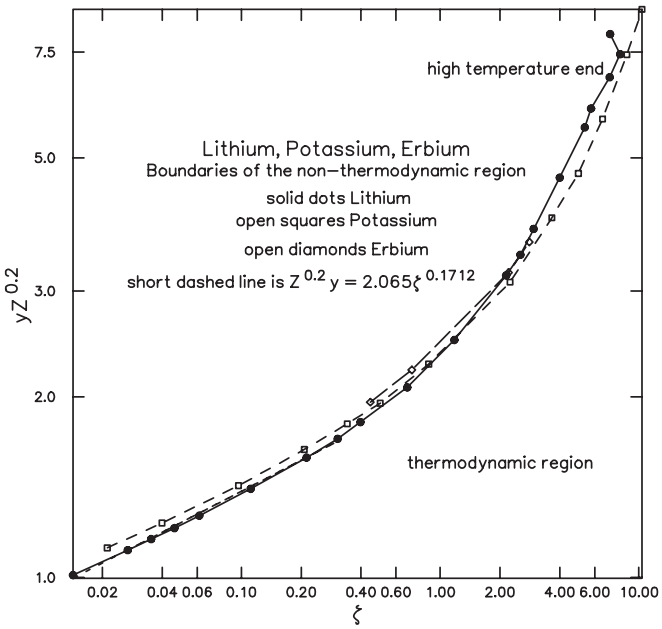

FIG. 7. Collapse of the data for the boundary of the nonthermodynamic region in the ζ-y plane. It is illustrated for lithium, potassium, and erbium. The short-dashed line is almost completely obscured by the solid line and it runs from the left border to $\zeta=0.3$.

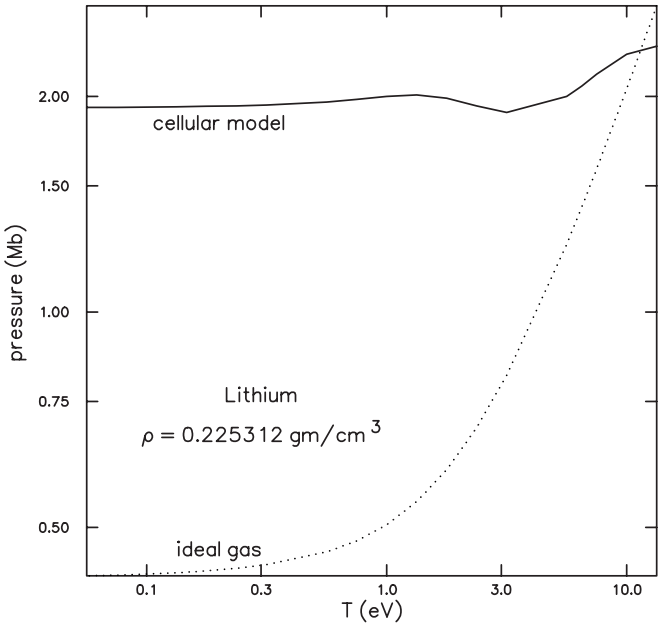

FIG. 8. Spherical cellular model pressure and the ideal Fermi gas pressure for lithium at fixed density as a function of temperature.

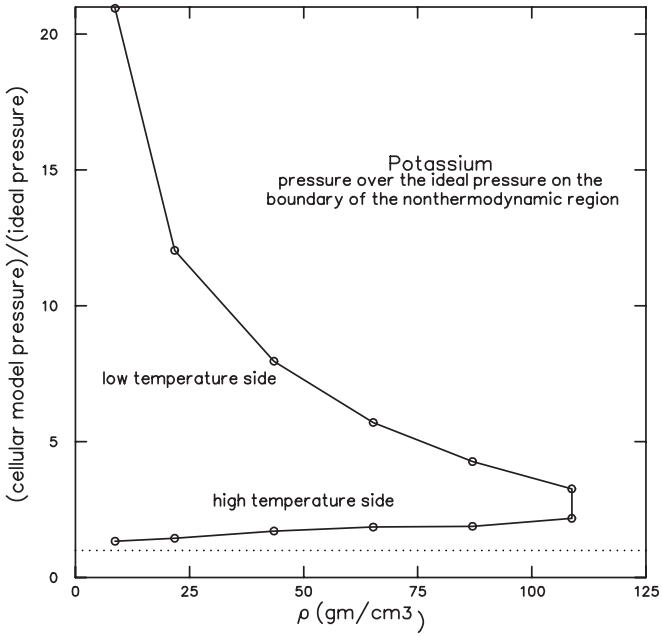

FIG. 10. Spherical cellular model temperature on the boundary of the nonthermodynamic region for potassium. The dotted line corresponds to a value of unity for the pressure ratio.

nonthermodynamic region, the two-phase region, and the region where the spherical cellular model pressure exceeds that of the ideal Fermi gas are shown for erbium in Fig. 9.

It is of interest to see the behavior of the pressure ratio on the boundary of the nonthermodynamic region. I illustrate this in Fig. 10 for potassium. There is very little overpressure on the high-temperature side in this case.υSince the nonthermodynamic behavior does not occur in hydrogen, I look to the following two approximations for an explanation of its occurrence. First, I have made the intra-atom independent

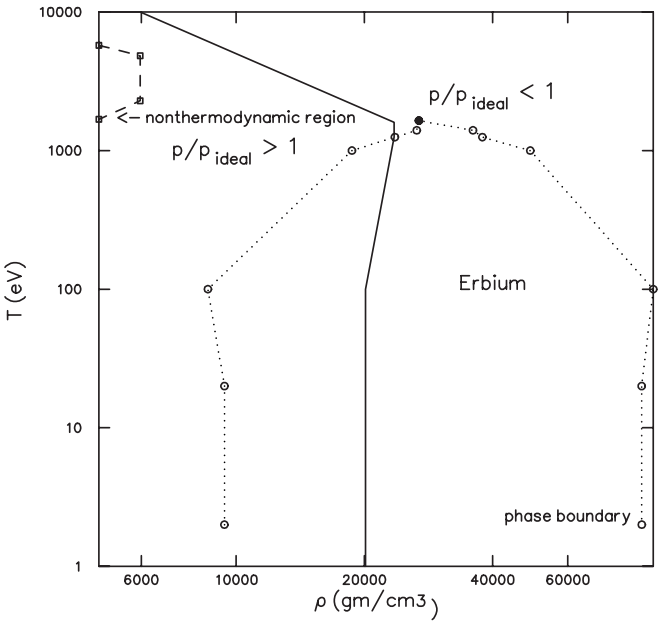

FIG. 9. Spherical cellular model for erbium showing the boundaries of the three regions.

electron approximation, (2.11). Second, instead of computing Z different potentials v by subtracting the contribution from $\mathcal{D}$ in (2.18) of the wave function of each state, I have computed by simply subtracting the $1/Z$ fraction of the total, thereby obtaining only one .

An important consideration is the fact that the solution using (2.10) for $\vec{k}=\vec{0}$ has no nonthermodynamic regions [21]. The difference between (2.10) for $\vec{k}=\vec{0}$ and $\vec{k}\neq\vec{0}$ is simply the addition of $\vec{k}$-dependent terms to the Hamiltonian and the multiplication of the wave function by a factor of $\Pi_{j=1}^{Z}\exp(i\vec{k}\cdot\vec{r}_j)$. These changes do not change the eigenvalues of the Schrödinger equation. In addition, they do not change the electron density either. Thus, while this result means that hydrogen is proven free from nonthermodynamic regions, this is not the case for the independent electron model (2.11) for $Z>1$. (Lieb's results [21] do not, of course, preclude the existence of two-phase regions.)

The region of overpressure occurs for small temperature and density. For this reason, I use as an illustration the behavior of the lowest $\epsilon(\vec{k}=\vec{0})$. If I do not include the $T(\partial\epsilon_j/\partial T)|_\Omega$ term in (2.5), then for temperatures small compared to the differences between the lowest eigenvalue and the next eigenvalue for (2.11) and (2.12), then the modified Eq. (2.5) gives the lowest ϵ.

The quantities on which the pressure depends [Eq. (2.4)] are the ϵ's. For lithium along the $T=0.5$ eV isotherm, I illustrate the lowest ϵ vs ρ in Fig. 11. The pressure is a sum of the contribution of the $\epsilon(\vec{k}=\vec{0})$'s and the integrals over the first Brillouin zone. These latter are like the kinetic energy. As is clear for Figs. 2 and 11, the derivative of $\epsilon(\vec{k}=\vec{0})$ is positive when $p/p_{\text{ideal}}>1$ and negative otherwise. This feature illustrates the mechanism which creates the overpressure.

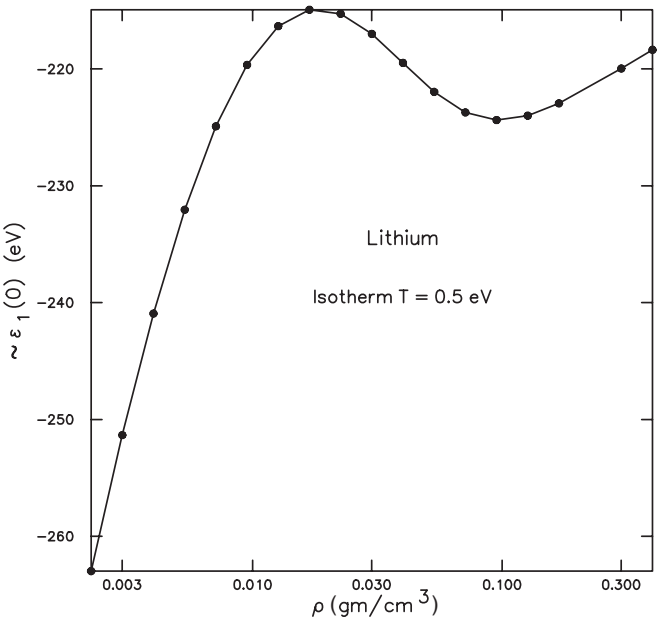

FIG. 11. The lowest $\epsilon(\vec{k}=\vec{0})$ versus density ρ.

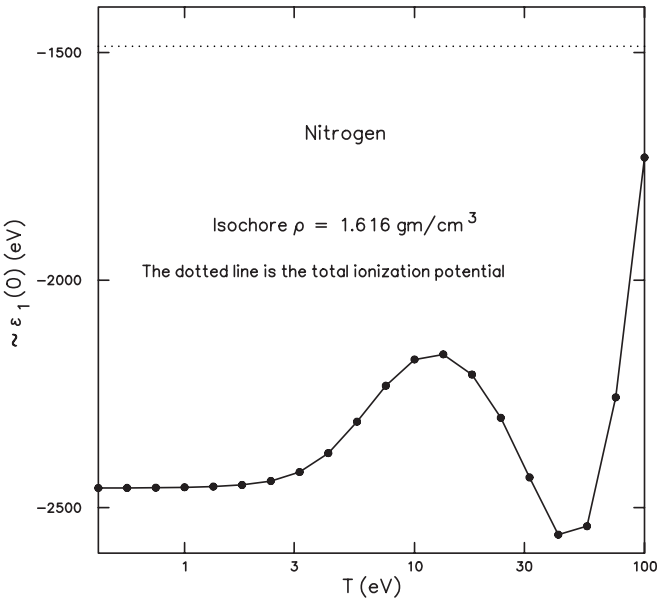

FIG. 12. Comparison of the lowest $\epsilon(\vec{k}=\vec{0})$ of the spherical cellular model and the experimental total ionization potential for nitrogen. The variation for $T>3$ eV is due to the dependence of the Schrödinger equation on y and ζ, which effects go to zero for small T.

Physically, at high densities, the energy eigenvalues are lowered because the electrons are forced to be close to the nucleus, and at low densities the energy eigenvalues decrease with decreasing densities as the volume constraint is removed (Fig. 11). This latter remark is valid when the temperature is not so high as to overwhelm the behavior illustrated by the lowest ϵ. Of course, at higher temperatures, the other eigenvalues contribute in an important way. Finally, physically, at very low densities, because of entropy, there is total ionization and p/p_{ideal} should go to unity.

The lowest value of ϵ is the lowest single-particle energy state which results from the intra-atom independent electron approxiation. This value of ϵ is to be compared with the total ionization energy. I have used the results of Moore [22]. An illustration of the comparison between the experimental data and the spherical cellular model data for nitrogen is shown in Fig. 12. The results for the spherical cellular model have settled down to the lowest ϵ within graphical accuracy for $T \leq 2$ eV. As can be seen in this figure, the intra-atom independent electron approximation used in the spherical cellular model leads to a much lower ϵ than the experimental total ionization energy. The independent electron approximation equation for $T \rightarrow 0$ is a Hartree-type equation. Figure 11 shows this equation to be inadequate. This inadequacy is what leads to the nonthermodynamic behavior.

At very low densities, the electron behavior as given by the independent electron approximation does not give a proper accounting of the electron-electron repulsion. As seen in the potassium electron density plot, Fig. 13, the predicted size of the potassium atom is much too small by about two orders of magnitude. The entire atom is almost completely inside one Bohr radius. In this type of case every electron in the independent electron approximation experiences the strong attraction near the nucleus, which leads to a much more negative potential energy than there should be, as shown in Fig. 12. So the electrons are moving very rapidly, which creates much too high a pressure. It is this feature, i.e., that the spherical cellular model maintains too small an atomic size, which accounts for the behavior seen in Fig. 8. The Thomas-Fermi model also leads to excessively high pressures as T goes to zero, but to a lesser extent.

I point out that at high densities one expects the electron distribution to be relatively uniform. Consequently the potential funciton should be about the same as that computed in

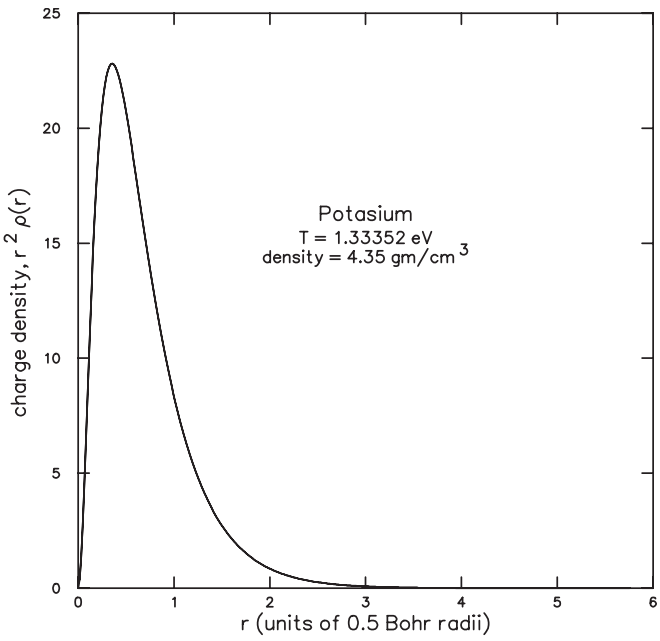

FIG. 13. Electron density, as a function of radius, for a sample of potassium.

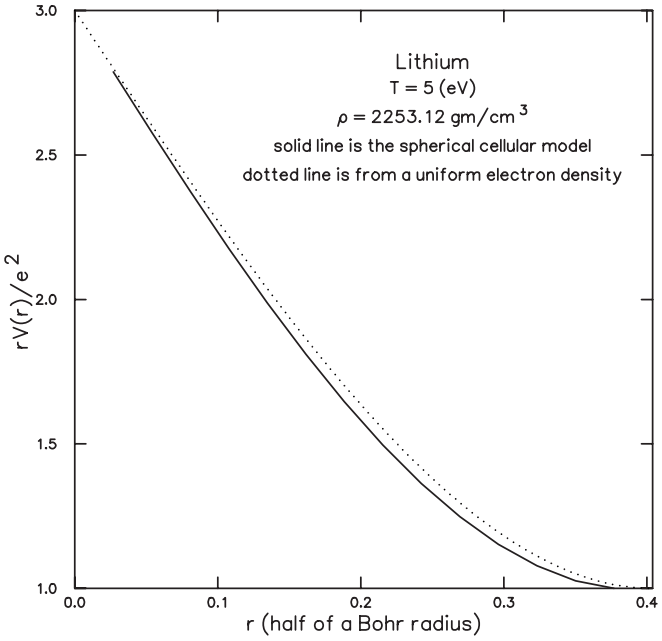

FIG. 14. Comparison of the single-electron potential given by the spherical cellular model and the analytical result for a uniform electron density.

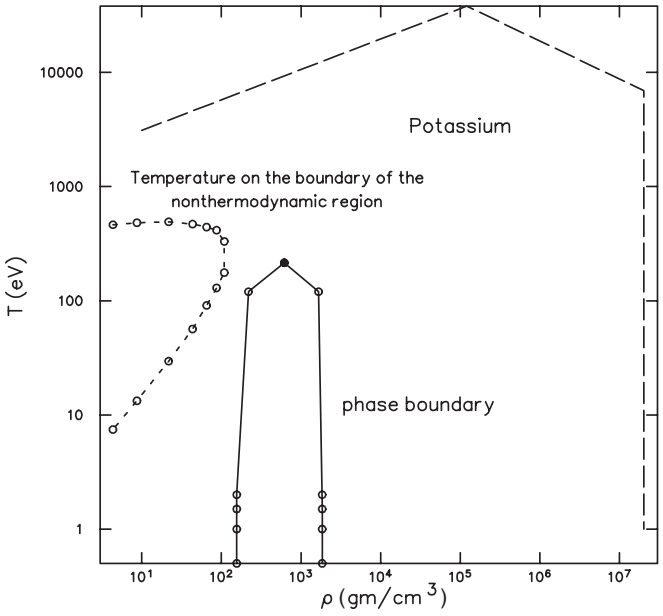

FIG. 15. The region above and to the right of the long dashed line is where the spherical cellular model agrees with the series results within 5%. The nonthermodynamic and the two-phase regions are also shown for potassium.

[2] for a uniform electron distribution. This result does indeed hold true as I illustrate in Fig. 14. The spherical cellular model results in this figure correspond to a small concentration of the electrons near the ion, which is not unreasonable. For low densities, the potential v drops much more rapidly with r because the electrons are no longer uniformly distributed but cluster near the ion.

I note [23] that the total experimental ionization energy (except for $Z=1$) is fitted fairly well (as far as the data goes [22]) by $I=14.82Z^{2.38}$. The ratio between the spherical cellular model results and the experimental data is fitted fairly well by the ratio $=1.55Z^{1/2}$, again except for $Z=1$

VI. CONCLUSIONS

Remember that it is a density derivative that leads to the pressure (2.4). So, since the pressure comes out right in this model for high density (see Fig. 2), the derivative of the lowest ϵ needs to be higher, so that the pressure is also higher. The location of this higher pressure is illustrated in Fig. 8 and the discussion of that figure. I conclude, in line with textbook thinking, that the intra-atom, independent electron approximation does not provide an adequate wave function in the low-density, low-temperature range.

There is, however, a region in which the spherical cellular model is valid within, say 5%, as reported by Baker and Johnson [24], who compared the results with the series expansion in the electric charge. The comparison is not in the region to be significantly affected by the correction [3]. They obtained the following results. There is a good comparison when

$$y \le 0.6\left(\frac{2}{1+Z}\right)^{1/12}\frac{\zeta^{1/9}}{Z^{1/12}}, \quad \zeta \le \zeta_1 = 0.486\,565\,2\left(\frac{2Z}{1+Z}\right)^{3/4},$$

$$y \le 0.65\frac{\zeta^{2/9}}{Z^{1/4}}, \quad \zeta_1 < \zeta < \zeta_2 = 1052.2742\left(\frac{2Z}{1+Z}\right)^{3/4},$$

$$y \le 0.3\left(\frac{1+Z}{2}\right)^{1/12}\frac{\zeta^{3/9}}{Z^{1/4}}, \quad \zeta_2 \le \zeta < 2.7\times 10^4\left(\frac{2Z}{1+Z}\right)^{3/4}. \tag{6.1}$$

The implication of these results is illustrated in Fig. 15. The spherical cellular model compares well with the series expansion above and to the right of the long-dashed curve. A comparison of the results of Figs. 6 and 14 suggests that good results for the spherical cellular model are probably obtained for densities a couple of orders of magnitude smaller than those indicated in Fig. 15. The authors of [24] indicate a very conservative approach.

I conclude that the spherical cellular model should give a reasonable approximation away from the two-phase region, the nonthermodynamic region, the region in which there is the formation of molecules, and of course the region of solids.

ACKNOWLEDGMENTS

The author would like to thank S. Crockett for some of the Thomas-Fermi data used in this paper. This work was carried out under the auspices of the National Nuclear Security Administration of the U.S. Department of Energy at the Los Alamos National Laboratory under Contract No. DE-AC52-06NA25396.

[1] G. A. Baker, Jr., Phys. Rev. E **56**, 5216 (1997).
[2] G. A. Baker, Jr., Phys. Rev. E **68**, 056112 (2003).
[3] G. A. Baker, Jr., Phys. Rev. E **75**, 059902(E) (2007).
[4] G. A. Baker, Jr. and J. D. Johnson, Physica A **265**, 129 (1999).
[5] G. A. Baker, Jr. and J. D. Johnson, Physica A **345**, 722 (2005).
[6] G. A. Baker, Jr. and J. D. Johnson, Physica A **359**, 345 (2006).
[7] G. A. Baker, Jr. and J. D. Johnson, Physica A **382**, 765 (2007).
[8] L. H. Thomas, Proc. Cambridge Philos. Soc. **23**, 542 (1927).
[9] E. Fermi, Rend. Accad. Naz. Lincei **6**, 602 (1927).
[10] R. P. Feynman, N. Metropolis, and E. Teller, Phys. Rev. **75**, 1561 (1949).
[11] E. Lieb, Rev. Mod. Phys. **53**, 603 (1981).
[12] L. Spruch, Rev. Mod. Phys. **63**, 151 (1991).
[13] S. Eliezer, A. Ghatak, and H. Hora, *Fundamentals of Equations of State* (World Scientific, Singapore, 2002).
[14] P. A. M. Dirac, Proc. Cambridge Philos. Soc. **26**, 376 (1930).
[15] R. D. Cowan and J. Ashkin, Phys. Rev. **105**, 144 (1957).
[16] G. A. Baker, Jr., J. Stat. Phys. **110**, 971 (2003).
[17] K. Huang, *Statistical Mechanics* (Wiley, New York, 1963).
[18] A. Y. Potekhin, G. Massacrier, and G. Chabrier, Phys. Rev. E **72**, 046402 (2005).
[19] G. A. Baker, Jr., Int. J. Mod. Phys. B **21**, 2045 (2007).
[20] P. Renaudin, C. Blancard, J. Clérouin, G. Faussurier, P. Noiret, and V. Recoules, Phys. Rev. Lett. **91**, 075002 (2003).
[21] E. Lieb, Rev. Mod. Phys. **48**, 553 (1976).
[22] C. E. Moore, *Ionization Potentials and Ionization Limits Derived from the Analysis of Optical Spectra*, Natl. Bur. Stand. Ref. Data Ser., Natl. Bur. Stand. (U.S.) Circ. No. 34 (U.S. GPO, Washington, D.C., 1970).
[23] J. D. Johnson (private communication).
[24] G. A. Baker, Jr. and J. D. Johnson, in *Condensed Matter Theories*, edited by S. Hernández and J. W. Clark (Nova Scientific, Huntington, NY, 2001), Vol. 16, p. 379.